PHYSICAL REVIEW A **89**, 021402(R) (2014)

Strong-field ionization of He by elliptically polarized light in attoclock configuration

I. A. Ivanov* and A. S. Kheifets†

Research School of Physical Sciences, The Australian National University, Canberra ACT 0200, Australia

(Received 29 September 2013; published 11 February 2014)

We perform time-dependent calculations of strong-field ionization of He by elliptically polarized light in configuration of recent attoclock measurements of Boge *et al*. [Phys. Rev. Lett. **111**, 103003 (2013)]. By solving a three-dimensional time-dependent Schrödinger equation, we obtain the angular offset θ_m of the maximum in the photoelectron momentum distribution in the polarization plane relative to the position predicted by the strong-field approximation. This offset is used in attoclock measurements to extract the tunneling time. Our calculations clearly support the set of experimental angular offset values obtained with the use of nonadiabatic calibration of the *in situ* field intensity, and disagree with an alternative set calibrated adiabatically. These findings are in contrast with the conclusions of Boge *et al*. who found a qualitative agreement of their semiclassical calculations with the adiabatic set of experimental data. This controversy may complicate interpretation of the recent attoclock measurements.

DOI: 10.1103/PhysRevA.89.021402 PACS number(s): 32.80.Rm, 32.80.Fb, 42.50.Hz

One of the recent advances in attosecond science was experimental observation of the time delay of photoemission after subjecting an atom to a short and intense laser pulse. Theoretical interpretation of such measurements depends on the Keldysh parameter γ which draws the borderline between the truly quantum multiphoton regime $\gamma > 1$ and a semiclassical tunneling regime $\gamma < 1$ [1]. The time delay measurements in the multiphoton regime by attosecond streaking [2] or two-photon sideband interference [3,4] can be conveniently interpreted by the Wigner time delay theory [5]. Even though some quantitative differences remain between measured and calculated time delays (see, e.g., [6]), qualitatively, these measurements are now well understood. At the same time, interpretation of the attosecond measurements in the tunneling regime by attosecond angular streaking [7,8] or high harmonics generation [9,10] is less straightforward. Indeed, the timing of the tunneling process has been a subject of numerous discussions and a long controversy (see [11] for a comprehensive review).

The attosecond angular streaking technique, termed colloquially as a tunneling clock or an attoclock, uses the rotating electric-field vector of the elliptically polarized pulse to deflect photoionized electrons in the angular spatial direction. Then the instant of ionization is mapped to the final angle of the momentum vector in the polarization plane, and a tunneling time is calculated using a semiclassical propagation model. By employing this technique, Eckle *et al*. [8] placed an intensity-averaged upper limit of 12 as on tunneling time in strong-field ionization of He with peak intensities ranging from 2.3 to 3.5 units of 10^{14} W/cm^2. In a subsequent paper by the same group [12], the attoclock was used to obtain information on the electron tunneling geometry and to confirm vanishing tunneling time. In addition, by comparing the angular streaking results in Ar and He, multielectron effects were clearly identified. Further on, the influence of the ion potential on the departing electron was considered and explained within a semiclassical model [13,14]. In a recent development [15], the attoclock technique was transferred from a cold-target recoil-ion momentum spectrometer (COLTRIMS) to a velocity map imaging spectrometer (VMIS). These refined attoclock measurements revealed a real and not instantaneous tunneling time over a large intensity regime [16]. Various competing theories of tunneling ionization were assessed against these experimental data, and some of them were found consistent with the data.

In the latest report [17], the attoclock measurements on He were used to assess the influence of nonadiabatic tunneling effects. In the tunneling regime, the electron tunnels adiabatically, it experiences a static field while tunneling, and exits the tunnel with zero momentum [1]. By employing both the COLTRIMS and VMIS techniques, the attoclock measurements of Ref. [17] were extended over a large range of intensities from one to eight units of 10^{14} W/cm^2, corresponding to a variation of the Keldysh parameter γ from 0.7 to 2.5. The upper end of the γ interval clearly trespasses on the multiphoton regime where the adiabatic hypothesis becomes questionable and the electron exits the tunnel with a nonzero momentum. Because this exit momentum is used as a tool for *in situ* calibration of the field intensity in the attoclock experiments, adopting either the adiabatic or nonadiabatic tunneling hypothesis would strongly affect the intensity calibration and the tunneling time results. In order to overcome this uncertainty, Boge *et al*. [17] performed a measurement of the angle of the photoelectron momentum at the detector defined by $\theta_m = \arctan(p_{x\ \mathrm{final}}/p_{y\ \mathrm{final}})$. Provided the electron is tunnel ionized at the maximum of the electric field E_x and is driven to the detector by the laser pulse, its final momentum is aligned with the vector potential at the moment of ionization A_y and hence $\theta_m = 0$. Nonzero values $\theta_m \neq 0$ can be attributed to the Coulomb field of the ionic core and/or a finite tunneling time

Boge *et al*. [17] obtained two sets of the offset angles θ_m under the two tunneling scenarios. Then they attempted to reproduce their data qualitatively with a TIPIS model (tunnel ionization in parabolic coordinates with induced dipole and Stark shift). The version of the model based on the nonadiabatic tunneling hypothesis predicted increasing of the offset angle with increase of the field intensity. Conversely,

*Igor.Ivanov@anu.edu.au
†A.Kheifets@anu.edu.au

the adiabatic model showed decrease of the offset with growing intensity, which was indeed the case experimentally. On this qualitative basis, Boge *et al.* [17] concluded that their experiments conformed to the adiabatic tunneling scenario. Quantitative difference of the adiabatic experimental data and theory was attributed to a finite tunneling time. Comparable difference between the nonadiabatic TIPIS theory and experiment can also be attributed to the same finite tunneling time effect [18].

In the present work, we perform accurate numerical calculations of the angular offset θ_m by solving a 3D time-dependent Schrödinger equation (TDSE). Our theoretical model is fully *ab initio*, it uses no adjustable parameters, and does not require any specific tunneling hypothesis. Results of our calculations support the set of experimental data calibrated under the nonadiabatic hypothesis. If this agreement is not accidental, it may indicate the influence of nonadiabatic effects predicted by the analytical theory [19]. It may also raise a question of validity of the TIPIS model and, more broadly, the interpretation of the tunneling time measurements reported in [16]. Indeed, our numerical results, the TIPIS model predictions, and the experimental data of Boge *et al.* [17] are mutually contradictory. The adiabatic tunneling scenario leads to the experimental data calibration which contradicts the present calculation. The nonadiabatic scenario leads to the TIPIS model prediction which is qualitatively incompatible with the experiment. One of the components of this triad, formed by the two theories and the experiment, is likely to be at fault.

Because of this important implication, we made every effort possible to verify our theoretical model and to validate our numerical computations. We tested the gauge invariance, partial wave and radial box convergence, and the carrier envelope phase (CEP) as well as the pulse length effects. All these tests were performed successfully.

We solve the TDSE for a helium atom described in a single active electron approximation:

$$i\,\partial\Psi(\boldsymbol{r})/\partial t = [\hat{H}_{\rm atom} + \hat{H}_{\rm int}(t)]\Psi(\boldsymbol{r}), \tag{1}$$

where $\hat{H}_{\rm atom}$ is the Hamiltonian of the field-free atom with effective one-electron potentials [20,21]. Two different model potentials were employed and produced indistinguishable results, which assured the accuracy of the calculation. The Hamiltonian $\hat{H}_{\rm int}(t)$ describes the interaction with the EM field. For this operator we can use both the length and velocity gauges:

$$\hat{H}_{\rm int}(t) = \begin{cases} \boldsymbol{E}(t)\cdot\hat{\boldsymbol{r}} \\ \boldsymbol{A}(t)\cdot\hat{\boldsymbol{p}}, \quad \boldsymbol{A}(t) = -\int_{-T_1/2}^{t}\boldsymbol{E}(\tau)\,d\tau. \end{cases} \tag{2}$$

The field is elliptically polarized in the xy plane with the components:

$$\begin{aligned} E_x &= \frac{\mathcal{E}\,f(t)}{\sqrt{1+\epsilon^2}}\cos(\omega t+\phi), \\ E_y &= \frac{\epsilon\mathcal{E}\,f(t)}{\sqrt{1+\epsilon^2}}\sin(\omega t+\phi). \end{aligned} \tag{3}$$

Here the ellipticity parameter $\epsilon = 0.87$ and the carrier frequency $\omega = 1.69$ eV (corresponding to the wavelength $\lambda =$ 735 nm) are the same as in the experimental work [16]. The pulse envelope was chosen to be $f(t) = \sin^2\pi t/T_1$, where $T_1 = 6T$ was the total pulse duration ($T = 2\pi/\omega$ is an optical period corresponding to the carrier frequency), and ϕ the CEP. The bulk of calculations was performed with $\phi = 0$ with a well-defined maximum of the vector potential relative to which the angular offset is measured. The electric field $\boldsymbol{E}$ and the vector potential $\boldsymbol{A}$ of this pulse are shown in Fig. 1. Some calculations at few selected field intensities were performed with varying ϕ. We also performed a separate set of calculations at varying field intensity for a shorter pulse with $T_1 = 3T$.

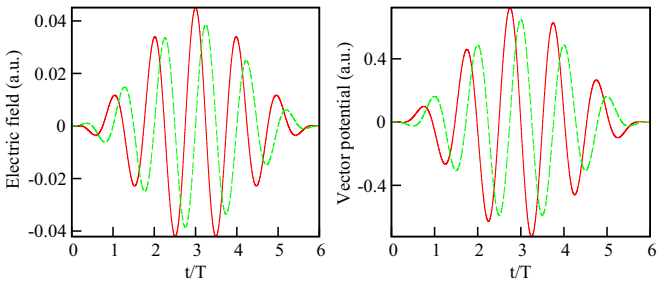

FIG. 1. (Color online) The electric field (left) and the vector potential (right) of the laser pulse with $\phi = 0$. Solid (red) line: x components; dashed (green): y components.

We seek a solution of Eq. (1) in the form of a partial wave expansion

$$\Psi(\boldsymbol{r},t) = \sum_{l=0}^{L_{\rm max}}\sum_{\mu=-l}^{l} f_{l\mu}(r,t)Y_{l\mu}(\theta,\phi). \tag{4}$$

The radial part of the TDSE is discretized on a spatial grid in a box. To propagate the wave function (4) in time, we use the matrix iteration method developed in [22] and further tested in calculations of strong-field ionization driven by linear [23,24] and circularly polarized [25] radiation.

By projecting the solution of the TDSE at the end of the laser pulse at $t = T_1$ on the set of the ingoing scattering states:

$$\psi_{\boldsymbol{k}}^{(-)}(\boldsymbol{r}) = \sum_{l\mu} i^l e^{-i\delta_l} Y_{l\mu}^*(\boldsymbol{n_k})Y_{l\mu}(\boldsymbol{n_r})R_{kl}(r) \tag{5}$$

(here $\boldsymbol{n_k} = \boldsymbol{k}/k$, and $\boldsymbol{n_r} = \boldsymbol{r}/r$ are unit vectors in the direction of $\boldsymbol{k}$ and $\boldsymbol{r}$, respectively), we obtain ionization amplitudes and the electron momentum distribution:

$$P(\boldsymbol{k}) = |\langle\psi_{\boldsymbol{k}}^{(-)}|\Psi(T_1)\rangle|^2. \tag{6}$$

For the field parameters that we considered, the ionization probabilities are extremely small (of the order of 10^{-10}) which required highly accurate computations. The issue of convergence and accuracy of the results was, therefore, critical for us in the present work. We found that convergence with respect to the number of partial waves retained in Eq. (4) is much faster in the velocity (V) gauge for the operator of the atom-field interaction (2). In the V gauge, a convergence on the acceptable level of accuracy was achieved for $L_{\rm max} = 40$ (laser intensity of 1.25×10^{14} W/cm^2 or less), $L_{\rm max} = 50$ for the intensity of 1.5×10^{14} W/cm^2, $L_{\rm max} = 60$ for the intensities in the range 1.75×10^{14} to 2.25×10^{14} W/cm^2,

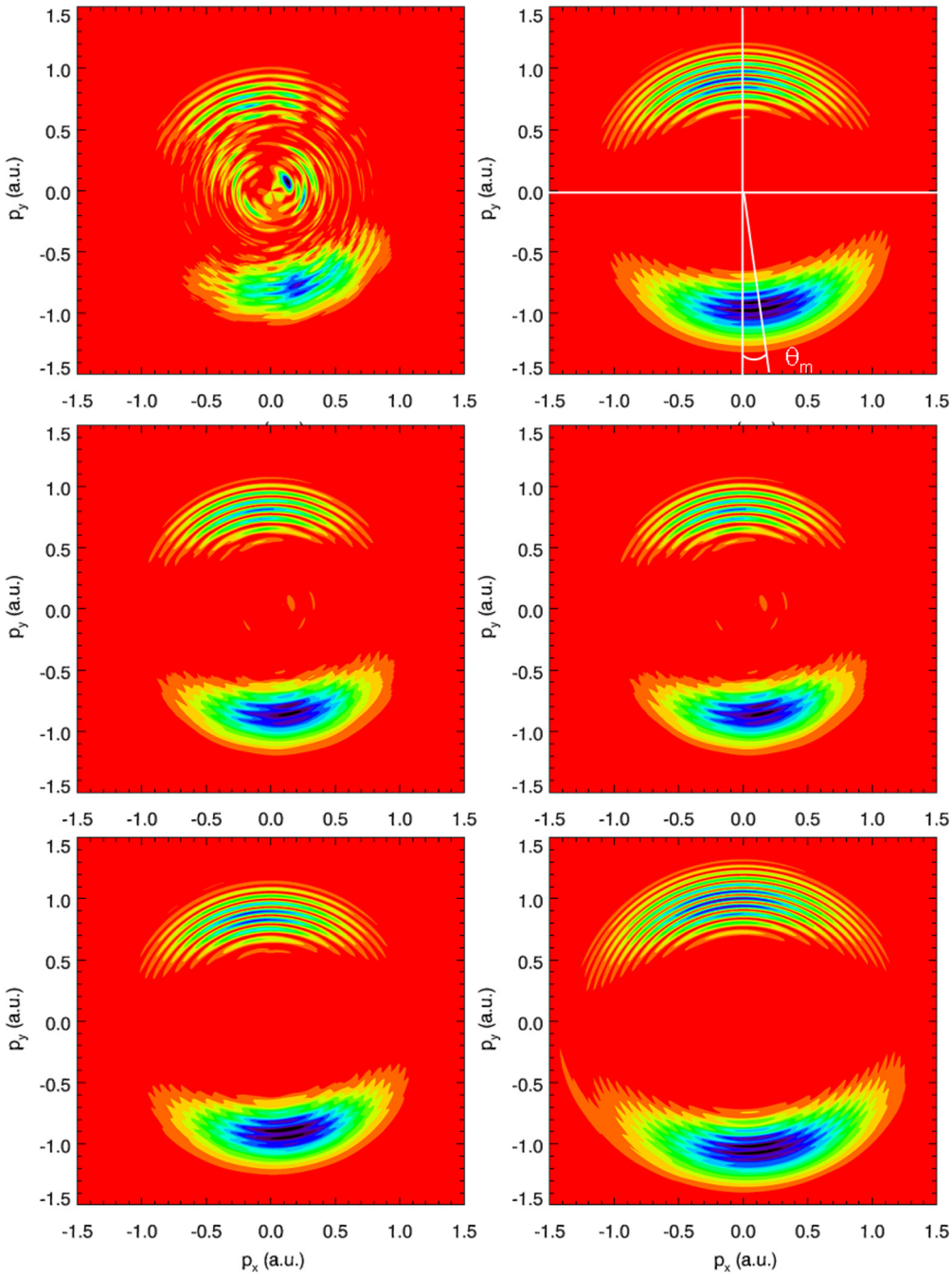

FIG. 2. (Color online) Photoelectron momentum distribution in the polarization plane for the field intensities of 1, 1.25, and 1.5 units of 10^{14} W/cm^2 (left set of panels, from top to bottom) and 1.75, 2, and 2.25 units of 10^{14} W/cm^2 (right set of panels, from top to bottom), $T_1 = 6T$, $\phi = 0$. The offset angle θ_m relative to the vertical $-p_y$ direction is visualized in the top right panel.

and $L_{\max} = 70$ for higher intensities. In comparison, for the intensity of 1.25×10^{14} W/cm^2, the L-gauge results begin to converge for $L_{\max}$ as large as 60. This made use of the L gauge for higher field intensities prohibitively expensive. Results reported below, therefore, have been obtained using the V gauge. Typical calculation required several hundred hours of CPU time, which was only possible by making our code run in parallel on a 1.2 petaflop supercomputer. A series of checks was performed to ensure convergence both with respect to the parameter $L_{\max}$, time integration step size Δt, and the box size $R_{\max}$. Some results of these checks are illustrated in Table I for the field intensity of 1.25×10^{14} W/cm^2. These checks allowed us to estimate the error margin of our calculation as 1°.

By using the projection operation (6), we calculate the electron momentum distribution in the polarization xy plane. These distributions are shown in Fig. 2 for the field intensities varying from 1×10^{14} to 2.25×10^{14} W/cm^2. Distributions were computed on a dense momenta grid in the $p_x p_y$ plane using the polar coordinates p and θ_p. To find the angular maximum θ_m, we integrated the momentum distribution over p and analyzed the resulting one-dimensional angular

TABLE I. Convergence with respect to the parameter L_{max} and the time integration step size Δt for the field intensity of 1.25×10^{14} W/cm^2, $T_1 = 3T$, and $\phi = 0$.

Computation parameters			Ionization probability
Gauge	L_{max}	Δt (a.u.)	10^{-10}
V	40	0.01	1.0235
V	50	0.01	1.0115
V	40	0.0075	1.0234
L	50	0.01	0.807
L	60	0.01	0.959

distribution. These distributions for varying field intensities are shown in Fig. 3. A similar procedure was followed in attoclock experiments.

The well-known strong-field approximation (SFA) [26] predicts that the direction of the maximum of the momentum distribution in the polarization plane should coincide with the direction of the vector potential $-\boldsymbol{A}(t_0)$ at the moment t_0 when the maximum field strength is attained. For the pulse with $T_1 = 6T$ and $\phi = 0$, $t_0 = 3T$, which is the midpoint of the laser pulse. The vector potential at this moment of time has zero x and positive y components (see the right panel of Fig. 1). The SFA predicts, therefore the zero offset angle $\theta_m = 0$ from the vertical $-p_y$ direction. Our TDSE calculations predict a noticeable offset θ_m relative to this direction which is visualized in the top right panel of Fig. 2.

For the laser intensity 1×10^{14} W/cm^2 (the left top panel of Fig. 2), one can still discern the structures in the momentum distribution reminiscent of the multiphoton regime. Nevertheless, the prominent global maximum predicted by the SFA is clearly visible. This maximum takes over completely at higher field intensities. Each multiphoton ring visible in Fig. 2 corresponds to an integer number of photons absorbed by the He atom $p_x^2 + p_y^2 = n\omega - 24.6$ eV. As we project the calculated 3D momentum distribution onto the p_x, p_y plane, we set $p_z = 0$. The multiphoton rings are not observed in the experiment, most probably because of the

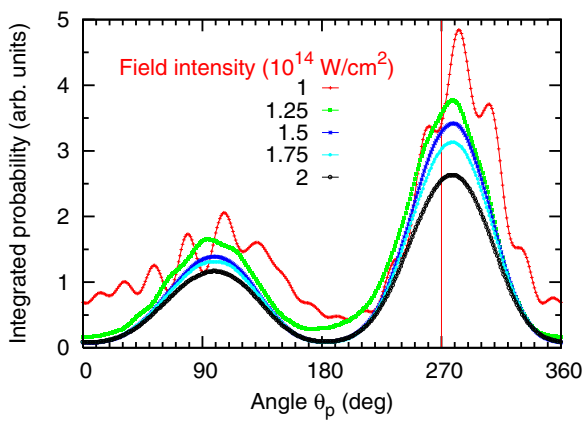

FIG. 3. (Color online) The radial p-integrated momentum distributions as the functions of the angle θ_p for field intensities of 1, 1.25, 1.5, and 1.75, and two units of 10^{14} W/cm^2. The CEP $\phi = 0$, pulse duration $T_1 = 6T$.

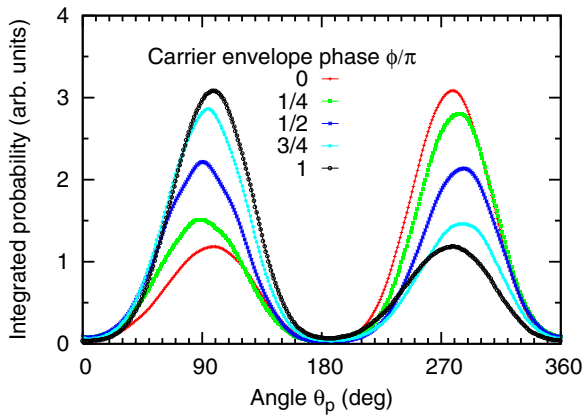

FIG. 4. (Color online) The radial p-integrated momentum distributions as the functions of the angle θ_p for CEP values $\phi = 0$, $\pi/4$, $\pi/2$, $3\pi/4$, and π. Field intensity 1.5×10^{14} W/cm^2.

finite range of p_z detected. Also, the experimental momentum distributions [12] show two symmetric lobes in the electron momentum distribution, whereas our calculations with $\phi = 0$ show two lobes of unequal strength. This asymmetry is due to the CEP variation investigated in [7,8] but not controlled in the later measurements [12,17]. We illustrate this asymmetry in Fig. 4 where we plot the p-integrated momentum distributions as functions of the angle θ_p for various CEP values. The relative intensity of the lobes in the second and fourth quadrants is changing with ϕ in exactly the same manner as observed in [7,8]. The figure shows some drift of the angular maximum position θ_m with ϕ. This is due to the drift of the direction of the vector potential at the maximum field strength, which is located at $t_0 = 3T$ when $\phi = 0$ but varies slightly for other ϕ values.

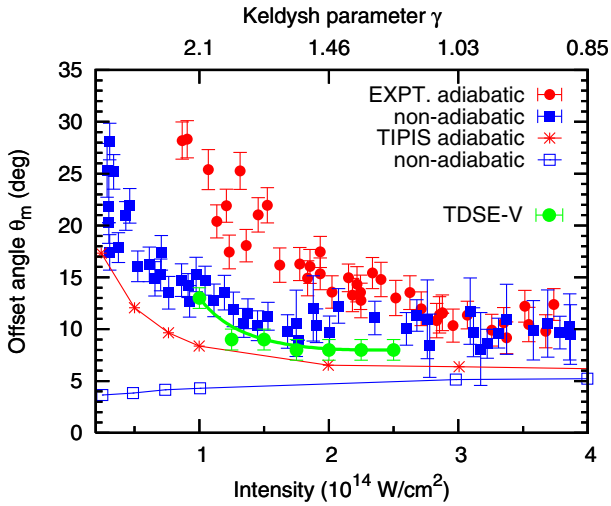

FIG. 5. (Color online) The offset angle θ_m of the photoelectron angular distribution from which the tunneling time is extracted. The two sets of the experimental data of Boge *et al.* [17] corresponding to the adiabatic and nonadiabatic field calibration are shown with the red filled circles and blue filled squares, respectively. The two analogous sets of the TIPIS calculations are shown with the red asterisks and blue open squares, respectively. The present TDSE results are shown with the green filled circles.

When the angular maximum values θ_m are compensated for this drift, they are all located at the same value (9°) irrespective of ϕ.

The offset from the SFA prediction $\theta_m = 0$ can be represented in the notations of Landsman *et al.* [16] as $\theta_m = \theta_{\rm Coul} + \omega\tau$. Here τ is the tunneling time; the angle $\theta_{\rm Coul}$ arises from the effect of the ionic potential [27] which is neglected in the SFA. The TIPIS model was used in the attoclock measurements [12,17] to evaluate the Coulomb contribution $\theta_{\rm Coul}$ and thus to evaluate the tunneling time τ.

Our numerical results for the angular offset θ_m, derived from Fig. 3 are shown in Fig. 5. In the same figure, we display two sets of the experimental data of Boge *et al.* [17] and their calculations using the semiclassical TIPIS model. Each set corresponds to either adiabatic or nonadiabatic *in situ* calibration of the field intensity. We see clearly that our TDSE calculations favor the set of experimental data calibrated nonadiabatically and strongly disagree with an alternative set of data calibrated adiabatically. At the same time, neither of the TIPIS calculations agree with the corresponding set of the experimental data. The adiabatic TIPIS set behaves qualitatively similar to the corresponding set of the experimental data, but numerically is much closer to the nonadiabatic set of the experimental data. The nonadiabatic TIPIS set is qualitatively different as it predicts the offset θ_m rising with an increasing field intensity.

If the agreement of the present calculation with the set of experimental offset angles, corresponding to the nonadiabatic calibration of the *in situ* field intensity, is not coincidental then we can draw the following conclusions: (i) nonadiabatic tunneling effects are noticeable and cannot be discarded and/or (ii) the TIPIS model is inaccurate and cannot be used to extract the tunneling time. The second conclusion has strong implications for the ongoing tunneling time debate.

The authors wish to thank Claudio Cirelli and Robert Boge for their detailed and extensive comment on the present work. Many discussions with Misha Ivanov, Olga Smirnova, and Alexandra Landsman were also very useful and stimulating. The authors acknowledge support from the Australian Research Council in the form of the Discovery grant, Grant No. DP120101805. Resources of the National Computational Infrastructure (NCI) Facility were employed.

[1] L. V. Keldysh, JETP USSR **47**, 1945 (1964) [Sov. Phys. JETP **20**, 1307 (1965)].
[2] M. Schultze *et al.*, Science **328**, 1658 (2010).
[3] K. Klünder *et al.*, Phys. Rev. Lett. **106**, 143002 (2011).
[4] D. Guénot *et al.*, Phys. Rev. A **85**, 053424 (2012).
[5] C. A. A. de Carvalho and H. M. Nussenzveig, Phys. Rep. **364**, 83 (2002).
[6] A. S. Kheifets, Phys. Rev. A **87**, 063404 (2013).
[7] P. Eckle *et al.*, Nat. Phys. **4**, 565 (2008).
[8] P. Eckle *et al.*, Science **322**, 1525 (2008).
[9] D. Shafir *et al.*, Nature (London) **485**, 343 (2012).
[10] M. Lein, Nature (London) **485**, 313 (2012).
[11] R. Landauer and T. Martin, Rev. Mod. Phys. **66**, 217 (1994).
[12] A. N. Pfeiffer *et al.*, Nat. Phys. **8**, 76 (2012).
[13] A. N. Pfeiffer, C. Cirelli, A. S. Landsman, M. Smolarski, D. Dimitrovski, L. B. Madsen, and U. Keller, Phys. Rev. Lett. **109**, 083002 (2012).
[14] C. Hofmann, A. S. Landsman, C. Cirelli, A. N. Pfeiffer, and U. Keller, J. Phys. B **46**, 125601 (2013).
[15] M. Weger, J. Maurer, A. Ludwig, L. Gallmann, and U. Keller, Opt. Express **21**, 21981 (2013).
[16] A. Landsman *et al.*, arXiv:1301.2766 (2013).
[17] R. Boge, C. Cirelli, A. S. Landsman, S. Heuser, A. Ludwig, J. Maurer, M. Weger, L. Gallmann, and U. Keller, Phys. Rev. Lett. **111**, 103003 (2013).
[18] C. Cirelli and R. Boge (private communication).
[19] G. L. Yudin and M. Y. Ivanov, Phys. Rev. A **64**, 013409 (2001).
[20] A. Sarsa, F. J. Gálvez, and E. Buendia, At. Data Nucl. Data Tables **88**, 163 (2004).
[21] A. E. S. Green, D. L. Sellin, and A. S. Zachor, Phys. Rev. **184**, 1 (1969).
[22] M. Nurhuda and F. H. M. Faisal, Phys. Rev. A **60**, 3125 (1999).
[23] A. N. Grum-Grzhimailo, B. Abeln, K. Bartschat, D. Weflen, and T. Urness, Phys. Rev. A **81**, 043408 (2010).
[24] I. A. Ivanov, Phys. Rev. A **83**, 023421 (2011).
[25] I. A. Ivanov and A. S. Kheifets, Phys. Rev. A **87**, 033407 (2013).
[26] A. M. Perelomov and V. S. Popov, Zh. Eksp. Teor. Fiz. **52**, 514 (1967) [Sov. Phys. JETP **25**, 336 (1967)].
[27] L. B. Madsen, L. A. A. Nikolopoulos, T. K. Kjeldsen, and J. Fernández, Phys. Rev. A **76**, 063407 (2007).